

Sparse Estimation in a Correlated Probit Model

Stephan Mandt^{*1}, Florian Wenzel^{*2}, Shinichi Nakajima³, John Cunningham⁴, Christoph Lippert⁵, and Marius Kloft²

¹Data Science Institute, Columbia University

²CS Department, Humboldt University of Berlin

³Berlin Big Data Center, Technical University Berlin

⁴Department of Statistics, Columbia University

⁵Human Longevity Inc.

Abstract

Among the goals of statistical genetics is to find associations between genetic data and binary phenotypes, such as heritable diseases. Often, the data are obfuscated by confounders such as age, ethnicity, or population structure. Linear mixed models are linear regression models that correct for confounding by means of correlated label noise; they are widely appreciated in the field of statistical genetics. We generalize this modeling paradigm to binary classification, where we face the problem that marginalizing over the noise leads to an intractable, high-dimensional integral. We present a scalable, *approximate* inference algorithm that lets us fit the model to high-dimensional data sets. The algorithm selects features based on an ℓ_1 -norm regularizer which are up to 40% less confounded compared to the outcomes of uncorrected feature selection, as we show. The proposed method also outperforms Gaussian process classification and uncorrelated probit regression in terms of prediction performance.

1 Introduction

Genetic association studies have emerged as an important branch of statistical genetics [24, 36]. The goal of this field is to find causal associations between high-dimensional vectors of *genotypes*, such as single nucleotide polymorphisms (SNPs), and observable outcomes or *phenotypes*. These phenotypes may be continuous or binary, an example being the outcome of a certain disease. Genetic associations are typically sparse: only selected genes are responsible for a phenotype of interest. Finding a small number of relevant positions in the genome among ten thousands of irrelevant genes is challenging. For various complex diseases, such as bipolar disorder or type 2 diabetes [11], these sparse signals are yet largely undetected [24], which is why these missing associations have been entitled the *The Dark Matter of Genomic Associations* [24].

Genetic associations can be spurious, unreliable, and unreproducible when the data are subject to confounding [20, 27, 26]. Confounding can stem from varying experimental

^{*}denotes equal contributions

conditions and demographics such as age, ethnicity, or gender [22]. The perhaps most important type of confounding in statistical genetics arises due to population structure [2], as well as similarities between closely related samples [22, 23, 18]. Ignoring such confounders can often lead to spurious false positive findings that cannot be replicated on independent data [21]. Correcting for such confounding dependencies is considered one of the greatest challenges in statistical genetics [37].

A popular approach of correcting for confounding in statistical genetics is based on linear mixed models [23]. These are linear regression models with multivariate noise, where the noise models relatedness between the samples as a source of confounding. These models simultaneously account for a sparse contribution from the linear weight vector, and a dense contribution from the noise which is marginalized out. This algorithm finds a sparse weight vector while automatically accounting for population stratification [20].

Although successful, linear mixed models have been restricted to the linear regression case. We generalize this modeling paradigm to the case of binary classification. Probit regression forms the basis of our approach [5], where we add an ℓ_1 -norm (Lasso) regularizer that guarantees that the resulting weight vectors are sparse [35]. However, in contrast to simple probit regression, the model contains a correlated multivariate noise variable that correlates the binary labels. We show that two popular methods result as limiting cases: ℓ_1 -norm probit regression (for uncorrelated noise), and Gaussian process (GP) probit classification [33] (when the linear weight vector is zero). Yet, this approach faces a technical challenge: simultaneous inference of the linear weight and the correlated noise becomes intractable in high dimensions. To solve this problem, we suggest a variational EM algorithm. We demonstrate that this lets us scale our method to high-dimensional data.

In an experimental study on genetic data, we show the superiority of our approach over other methods. Compared to simple probit regression, our sparse features are up to 40% less correlated with the first principal component of the noise covariance that represents the confounder. Furthermore, compared to the linear mixed model Lasso [32], probit regression, and GP classification [33], our approach yields up to 5 percentage points higher prediction accuracies. In a computer malware experiment we show that our approach generalizes beyond statistical genetics.

Our paper is organized as follows. We separate modeling from inference. Section 2 is about modeling. We first review the confounding problem in binary classification and introduce two versions of our model: a simplified version based on a maximum-likelihood estimate of the noise variable, and the fully correlated model. Section 3 then contains the mathematical details of the inference procedure. In section 4 we apply our method to extract features associated with diseases and traits from confounded genetic data. We also test our method on a data set that contains a mix of different types of malicious computer software data.

2 Correlated Probit Regression

We first review the problem of confounding by population structure in statistical genetics in section 2.1. In section 2.2, we review linear mixed models and introduce a corresponding model for classification. We discuss the choice of the noise kernel in section 2.3 and connect to other models in section 2.4.

2.1 Confounding and similarity kernels

The problem of confounding is fundamental in statistics. A confounder is a common cause both of the genotypes and the traits. When it is unobserved, it induces spurious correlations that have no causal interpretation: we say that the genotypes and traits are *confounded* [20, 27, 26].

In statistical genetics, a major source of confounding originates from population structure [2]. Population structure implies that due to common ancestry, genes of individuals that are related co-inherit a large number of genes, making them more similar to each other, whereas the genes of people of unrelated ancestry are obtained independently, making them more dissimilar. For this reason, collecting genetic data has to be done with care. For example, when data is collected only in selected geographical areas (such as in specific hospitals), one thereby introduces a selection bias into the sample, meaning that the collected genes do not represent the overall population. This can heavily distort the prediction quality of a classifier. Unfortunately, many modern genetic data sets are confounded [37].

Another problem is that people who live geographically close often share other factors, such as similar environmental factors or culture. This, in turn, can lead to similar phenotypes (such as overweight, drinking habits, or diabetes). Thus, because genes correlate with geographic location and location may correlate with specific phenotypes, there is a resulting correlation between genes and these phenotypes that does not have a causal interpretation—another manifestation of confounding by population structure. It is an active area of research to find models that are less prone to confounding [37]. In this paper, we present such a model for the setup of binary classification.

A popular approach to correcting for confounding relies on similarity kernels, or kinship matrices [2]. Given n samples, we can construct an $n \times n$ matrix K that quantifies the similarity between samples based on some arbitrary measure. In the case of confounding by population structure, one typically chooses $K_{ij} = X_i^\top X_j$, where $X_i \in \mathbb{R}^d$ is a vector of genetic features of individual i . As $K \in \mathbb{R}^{n \times n}$ contains the scalar products between the genetic vectors of all individuals, it is a sensible measure of genetic similarity. As another example, when correcting for confounding by age, then we can choose K to be a matrix that contains 1 if two individuals have the same age, and zero otherwise. Details of constructing similarity kernels can be found in [2]. Next, we explain how the similarity matrix can be used to correct for confounding.

2.2 Generalizing linear mixed models

We first review the linear mixed model (LMM) of statistical genetics [23, 32]. LMMs are linear regression models that capture dependencies between the data points in terms of correlated noise. Consider the following class of generalized regression models which have an inverse link function f that relates the predictor variables and the noise with the observed outcomes:

$$y_i = f(X_i^\top w + \epsilon_i), \quad \epsilon = (\epsilon_1, \dots, \epsilon_n)^\top \sim \mathcal{N}(0, \Sigma). \quad (1)$$

To obtain the linear mixed model, we set $f \equiv \text{Id}$, denoting the identity. The outputs y_i may be continuous or discrete, and X_i is a set of n input variables. The variables ϵ_i are noise variables. Crucially, they are correlated and have a covariance Σ that is based on a

similarity kernel K ,

$$\Sigma = \lambda_1 \mathbf{I} + \lambda_2 K \quad (2)$$

The diagonal noise contribution is necessary to regularize the problem. The parameter $\lambda = (\lambda_1, \lambda_2)$ is found by cross-validation. In practice, we may use multiple similarity kernels.

Models of the above type allow for two different explanations of the observed outputs y . One explanation arises through the linear effect that we want to estimate. The other explanation arises through correlated noise. By construction, the noise covariance Σ contains information about similarities between the samples. The computational goal is to distinguish between these two effects.

Linear mixed models allow to efficiently do inference by preprocessing the data matrix by means of a rotation. To see this, assume $f \equiv \text{Id}$. We can always decompose the noise covariance as $\Sigma = UDU^\top$, where U is orthogonal and D is a diagonal matrix of eigenvalues of Σ . If we define $R = D^{-1/2}U^\top$, we can write the generalized linear mixed model as

$$Ry_i = RX_i^\top w + \tilde{\epsilon}_i, \quad \tilde{\epsilon} \sim \mathcal{N}(0, \mathbf{I}). \quad (3)$$

Thus, after preprocessing, the remaining model is simply a linear regression model that can be treated with standard tools. This is the basic idea behind LMMs.

However, when the inverse link function is not the identity, this methodology can not be used. In particular, we made use of the relation $R \circ f = f \circ R$, hence that the inverse link function commutes with the rotation. This is only true for the identity but not for a generic function f . For this reason, inference for generalized linear mixed models is much more complicated. We therefore need new inference algorithms when generalizing this modeling paradigm beyond linear regression.

In this paper we generalize the LMM modeling paradigm to a non-linear setup. We focus on the important class of binary classification problems [5, 16]. In the following, we assume $f \equiv \text{sign}$ which is the sign (or probit) function. This involves binary labels $y_i \in \{+1, -1\}$. As before, we break the independence of the label noises. This leads to the following model:

$$y_i = \text{sign}(X_i^\top w + \epsilon_i), \quad \epsilon = (\epsilon_1, \dots, \epsilon_n)^\top \sim \mathcal{N}(0, \Sigma). \quad (4)$$

In the special case of $\Sigma = \mathbf{I}$, this is just the probit model for classification. Because the binary labels are correlated in Eq. 4, we call this model the *correlated probit regression* model (CPR). Since we seek to optimize over w while marginalizing over the noise, our first goal is to derive a corresponding objective function.

To simplify the notation, we will without loss of generality assume that *all observed binary labels y_i are 1*. The reason why this assumption is no constraint is that we can always perform a linear transformation to absorb the sign of the labels into the data matrix and noise covariance (this transformation is shown in Appendix A). Thus, when working with this transformed data matrix and noise covariance, our assumption is satisfied.

Under our assumption, the likelihood function is the probability that all transformed labels are 1. This is satisfied when $X_i^\top w + \epsilon_i > 0$. When integrating over all realizations of noise, the resulting (marginal) likelihood is

$$\mathbb{P}(\forall i : y_i = 1 | w) = \mathbb{P}(\forall i : X_i^\top w + \epsilon_i > 0 | w) = \int_{\mathbb{R}_+^n} \mathcal{N}(\epsilon; X^\top w, \Sigma) d^n \epsilon. \quad (5)$$

The marginal likelihood is hence an integral of the multivariate Gaussian over the positive orthant. In section 3, we will present efficient approximations of this integral. Before we get there, we further characterize the model.

Next, we turn the correlated probit model into a model for feature selection. We are interested in a point estimate of the weight vector w that is sparse, i.e. contains zeros almost everywhere. This is well motivated in statistical genetics, because generally only a small number of genes are believed to be causally associated with a phenotype such as a disease. Sparsity is achieved using the Lasso [35], where we add an ℓ_1 -norm regularizer to the negative marginal likelihood:

$$\mathcal{L}(w) = -\log \int_{\mathbb{R}_+^n} \mathcal{N}(\epsilon; X^\top w, \Sigma) d^n \epsilon + \lambda_0 \|w\|_1^1. \quad (6)$$

The fact that the noise variable ϵ and the weight vector w have different priors or regularizations makes the model identifiable and lets us cleanly distinguish between linear effects and effects of correlated noise. In Appendix B we prove that the objective function Eq. 6 is convex.

2.3 Maximum a posteriori approximation

We now explore a formulation of the model that sheds light on the role of the noise kernel. For simplicity, we consider the simplest and most widely used covariance matrix Σ , which is a combination of diagonal noise and a linear kernel of the data matrix,

$$\Sigma = \lambda_1 \mathbf{I} + \lambda_2 X^\top X. \quad (7)$$

The linear kernel $X^\top X$ measures similarities between genes and therefore models the effect of genetic similarity between samples due to population structure. To motivate the choice of this kernel, we use a Gaussian integral identity:

$$\begin{aligned} \mathcal{L}(w) &= -\log \int_{\mathbb{R}_+^n} \mathcal{N}(\epsilon; X^\top w, \lambda_1 \mathbf{I} + \lambda_2 X^\top X) d^n \epsilon + \lambda_0 \|w\|_1^1 \\ &= -\log \int_{\mathbb{R}^d} dw' \mathcal{N}(w'; 0, \lambda_2 \mathbf{I}) \int_{\mathbb{R}_+^n} d^n \epsilon \mathcal{N}(\epsilon; X^\top (w + w'), \lambda_1 \mathbf{I}) + \lambda_0 \|w\|_1^1. \end{aligned} \quad (8)$$

We have introduced the new Gaussian noise variable w' . Conditioned on w' , the remaining integrals factorize over n . However, since w' is unobserved (hence marginalized out), it correlates the samples. We interpret w' as a confounder.

The simplest approximation to the log-likelihood Eq. 8 is to substitute the integral over w' by its maximum a posteriori (MAP) value:

$$\mathcal{L}(w, w') = -\sum_{i=1}^n \log \Phi \left(\frac{X_i^\top (w + w')}{\sqrt{\lambda_1}} \right) + \frac{1}{2\lambda_2} \|w'\|_2^2 + \lambda_0 \|w\|_1^1. \quad (9)$$

Above, $\Phi(\cdot)$ is the cumulative standard normal distribution function. Under the MAP approximation, the likelihood contribution to the objective function becomes symmetric in w and w' : only the sum $w + w'$ enters. The difference between the two weight vectors w and

w' in this approximation is only due to the different regularizers: while w' has an ℓ_2 -norm regularizer and is therefore dense, w is ℓ_1 -norm regularized and therefore sparse.

Under the MAP approximation, every feature gets a small non-zero weight from w' , and only selected features get a stronger weight from w . The idea is that w' models the population structure, which affects all genes. In contrast, we are interested in learning the sparse weight vector w , which has a causal interpretation because it involves only a small number of features.¹

The MAP approximation is computationally more convenient, but less powerful. Under the MAP approximation we optimize over w' , such that the objective function factorizes over n . This means that we have broken the correlations between the samples, which comes at the cost of reduced prediction performance. In contrast, in the original correlated probit model in Eq. 4, w' is marginalized out. This is more expensive, but generalizes better to unseen data. We compare of both approaches empirically in section 4.

2.4 Connection to other models

Before we come to inference, we point out how our approach connects to other methods. When removing the probit likelihood, the model becomes the linear mixed model Lasso (LMM-Lasso) by [32], hence $\mathbb{P}(Y|w) = \mathcal{N}(Y; X^\top w, \Sigma)$. This model has shown to improve selection of true non-zero effects as well as prediction quality [32]. Our model is a natural extension of the model by [32] to binary outcomes, such as the disease status of a patient. As we explain in this paper, inference of our model is, however, much more challenging than in [32].

Furthermore, by construction, our model captures two limiting cases: uncorrelated probit regression and Gaussian process (GP) classification. To obtain uncorrelated probit regression, we simply set the parameters $\lambda_i = 0$ for $i \geq 2$, thereby eliminating the non-diagonal covariance structure. To obtain GP classification, we simply omit the fixed effect (i.e., we set $w = 0$) so that our model likelihood becomes $\mathbb{P}(Y = Y^{\text{obs}}|w) = \int_{\mathbb{R}_+^n} \mathcal{N}(\epsilon; 0, \Sigma) d^n \epsilon$, where hence the noise variable ϵ plays the role of the latent function f in GPs [33]. When properly trained, our model will therefore outperform both approaches in terms of accuracy. We will compare our method to all three limiting cases in the experimental part of the paper and show enhanced accuracy.

3 Inference

In this section, we derive an algorithm to optimize the objective function of CPR in Eq. 6. This goal comes along with two major problems:

1. The ℓ_1 -norm regularizer for feature selection is not differentiable everywhere.
2. The likelihood contains an intractable, high-dimensional integral.

Our solution relies on a EM-type algorithm [13]. In the outer loop (the M-step), we follow gradients to optimize the objective. Since this objective function has an ℓ_1 -norm regularizer,

¹Note that the interplay of two weight vectors is different from an elastic net regularizer.

we have to split this outer optimization routine into two parts, one that optimizes the likelihood and one that optimizes the regularizer. This is described in 3.1. The inner loop (the E-step) consists of computing the gradient and the Hessian of the likelihood term by means of approximate inference, which is described in Sections 3.2 and 3.3. (Prediction in our model is addressed in Appendix C.)

3.1 M-step

The ℓ_1 -norm in the objective function in Eq. 6 prevents us from directly applying gradient based methods such as Newton’s method. A solution is given by the alternating direction method of multipliers (ADMM) [7] that involves a generalized objective:

$$\mathcal{L}(w, z, \eta) := -\log \int_{\mathbb{R}_+^N} \mathcal{N}(\epsilon; X^\top w, \Sigma) d^n \epsilon + \lambda_0 \|z\|_1 + \eta^\top (w - z) + \frac{1}{2} c \|w - z\|_2^2.$$

We minimize over w and z and maximize over η . In alternating between the minimization updates for w , z and a gradient step in η , we solve the original problem [7]. While the updates for z and η have analytic solutions, we compute the updates for w by numerical optimization. The part of the ADMM objective $\mathcal{L}(w, z, \eta)$ depending on w , called $\mathcal{L}(w)$ for brevity, is effectively ℓ_2 -norm regularized, enabling us to compute the gradient and the Hessian. This allows us to apply Newton’s Method to obtain the ADMM update in w .

3.2 E-step

The inner loop of the EM-algorithm amounts to computing the gradient and Hessian of $\mathcal{L}(w, z, \eta)$. These are not available in closed-form, but in terms of the first and second moment of a truncated Gaussian density.

Since computing the derivatives of the linear and quadratic term is straightforward, we focus on $\mathcal{L}_0(w) := -\log \int_{\mathbb{R}_+^N} \mathcal{N}(\epsilon; X^\top w, \Sigma) d^n \epsilon$, which contains the intractable integral. In the following, we use the short hand notation

$$\mu \equiv \mu(w) = X^\top w. \quad (10)$$

It is convenient to introduce the following probability distribution:

$$p(\epsilon | \mu, \Sigma) = \frac{\mathbb{1}[\epsilon \in \mathbb{R}_+^n] \mathcal{N}(\epsilon; \mu, \Sigma)}{\int_{\mathbb{R}_+^n} \mathcal{N}(\epsilon; \mu, \Sigma) d^n \epsilon}. \quad (11)$$

Above, $\mathbb{1}[\cdot]$ is the indicator function. This is just the multivariate Gaussian, truncated and normalized to the positive orthant; we call it the *posterior* distribution. We furthermore introduce

$$\begin{aligned} \mu_p(w) &= \mathbb{E}_{p(\epsilon | \mu(w), \Sigma)} [\epsilon], \\ \Sigma_p(w) &= \mathbb{E}_{p(\epsilon | \mu(w), \Sigma)} [(\epsilon - \mu_p(w))(\epsilon - \mu_p(w))^\top]. \end{aligned} \quad (12)$$

This is just the mean and the covariance of the *truncated* multivariate Gaussian, as opposed to μ, Σ which are the mean and covariance of the non-truncated Gaussian.

In the following we abbreviate $\mu_p \equiv \mu_p(w)$ and $\Sigma_p \equiv \Sigma_p(w)$, and write $\Delta\mu = \mu_p - \mu$ for the difference between the means of the posterior (the truncated Gaussian) and the un-truncated Gaussian. The gradient and Hessian of $\mathcal{L}_0(w)$ are given by

$$\begin{aligned}\nabla_w \mathcal{L}_0(w) &= \Delta\mu \Sigma^{-1} X^\top, \\ H_0(w) &= -X[\Sigma^{-1}(\Sigma_p - \Delta\mu \Delta\mu^\top) \Sigma^{-1} - \Sigma^{-1}] X^\top.\end{aligned}\tag{13}$$

Proofs are given in Appendix D. Note that the variable w enters through $\Sigma_p(w)$ and $\Delta\mu(w)$. Next, we describe how we approximate the intractable expectations involved in Eq. 13.

3.3 Approximate posterior inference

In Eq. 13 we have expressed the gradient and Hessian of $\mathcal{L}_0(w)$ in terms of the first and second moment of the posterior, Eq. 11. The problem is that computing the moments involves intractable expectations over this distribution. We employ expectation propagation (EP) [12] to approximate these expectations. Note that also other approximate inference schemes are possible, such as variational inference or sampling methods [33].

EP approximates moments of the posterior $p(\epsilon|\mu, \Sigma)$ in terms of a variational distribution $q(\epsilon)$, approximately minimizing the Kullback-Leibler divergence,

$$q^*(\epsilon|\mu_{q^*}, \Sigma_{q^*}) = \arg \min_q (\mathbb{E}_p[\log p(\epsilon|\mu, \Sigma)] - \mathbb{E}_p[\log q(\epsilon|\mu_q, \Sigma_q)]). \tag{14}$$

The variational distribution $q^*(\epsilon)$ is an un-truncated Gaussian $q^*(\epsilon; \mu_{q^*}, \Sigma_{q^*}) = \mathcal{N}(\epsilon; \mu_{q^*}, \Sigma_{q^*})$, characterized by the variational parameters μ_{q^*} and Σ_{q^*} . We approximate the mean and covariance of the posterior p in terms of the variational distribution, $\mu_p \approx \mu_{q^*}$, and $\Sigma_p \approx \Sigma_{q^*}$. We warm-start each gradient computation with the optimal parameters of the earlier iteration.

Algorithm 1 summarizes our procedure. We denote the expectation propagation algorithm for approximating the first and second moment of the truncated Gaussian by $\text{EP}(\mu, \Sigma)$. Here, μ and Σ are the mean and covariance matrix of the un-truncated Gaussian. The subroutine returns the first and second moments of the truncated distributions μ_q and Σ_q . When initialized with the outcomes of earlier iterations, this subroutine converges within a single EP loop.

Our algorithm thus consists of three nested loops; the outer ADMM loop, containing the Newton optimization loop for computing the update in w and the inner EP loop, which computes the moments of the posterior. We choose *stopping criterion 1* to be the convergence criterion proposed by Boyd [7] and choose *stopping criterion 2* to be always fulfilled, i.e. we perform only one Newton optimization step in the inner loop. Our experiments showed that doing only one Newton optimization step, instead of executing until convergence, is stable and leads to great speed improvements. ADMM is known to converge even when the minimizations in the ADMM scheme are not carried out exactly (see e.g. [15]).

3.4 Inference in the MAP approximated model

We briefly describe the optimization algorithm used for the MAP-approximated model. Recall that we aim to minimize the objective function, Eq. 9 jointly in (w, w') . For this

Algorithm 1 Sparse Correlated Probit Regression

```

 $X = y \circ \tilde{X}$   $\backslash\backslash$ pre-process the data
 $\Sigma = \text{diag}(y) \tilde{\Sigma} \text{diag}(y)$ 
repeat
   $\backslash\backslash$ get  $w^{k+1}$  by EP and Newton's Method
  initialize  $w = w^k$ 
  repeat
     $(\mu_q, \Sigma_q) \leftarrow \text{EP}(X^\top w, \Sigma)$ 
     $\Delta\mu = \mu_q - X^\top w$ 
     $g = \Delta\mu^\top \Sigma^{-1} X^\top + c(w - z^k + \eta^k)^\top$ 
     $H = X[\Sigma^{-1} - \Sigma^{-1}(\Sigma_q - \Delta\mu\Delta\mu^\top)\Sigma^{-1}]X^\top + c\mathbf{I}$ 
     $w = w - \alpha_t H^{-1}g$ 
  until criterion 2
   $\backslash\backslash$ ADMM updates
   $w^{k+1} = w$ 
   $z^{k+1} = S_{\lambda/c}(w^{k+1} + \eta^k)$   $\backslash\backslash$ soft thresholding, see Boyd [7]
   $\eta^{k+1} = \eta^k + w^{k+1} - z^{k+1}$ 
until criterion 1

```

purpose we introduce a block coordinate descent scheme alternating between updates in w and w' . The gradient of $\mathcal{L}(w, w')$ with respect to w' is given by

$$\nabla_{w'} \mathcal{L}(w, w') = - \sum_{i=1}^n \log \frac{\mathcal{N}(\lambda_1^{-\frac{1}{2}} X_i^\top (w + w'))}{\Phi(\lambda_1^{-\frac{1}{2}} X_i^\top (w + w'))} X_i^\top + \frac{1}{\lambda_2} w'^\top, \quad (15)$$

where $\mathcal{N}(\cdot)$ denotes the standard normal density. For updating w' we use gradient descent, while for updating w we employ ADMM (c.f. section 3.1).

For optimizing the MAP probit objective, Eq. 9, we alternate between a gradient step in w' and an ADMM step in w . This procedure can be made faster by using a second-order optimization method for obtaining the updates in w' .

4 Empirical Analysis and Applications

We studied the performance of our proposed methods in experiments on both artificial and real-world data. We considered the two versions of our model: CPR (the full correlated probit model as specified in Eq. 8) and CPR-MAP (its MAP approximation as contained in Eq. 9). Our data was taken from the domains of statistical genetics and computer malware prediction. Our achievements can be summarized as follows:

- We compare against 3 competing methods, including uncorrelated probit regression, GP classification and the LMM Lasso. In all considered cases, CPR achieves higher classification performance.
- The features that our algorithm finds are up to 40% less confounded by population structure.

- CPR outperforms its MAP approximation across all considered datasets. Yet, in many cases CPR-MAP is a cheap alternative to the full model.

4.1 Experimental setup

For the real-world and synthetic experiments, we first need to make a choice for the class of kernels that we use for the covariance matrix. We choose a combination of three contributions,

$$\Sigma = \lambda_1 \mathbf{I} + \lambda_2 X^\top X + \lambda_3 \Sigma_{\text{side}}. \quad (16)$$

The third term is optional and depends on the context; it is a kernel that we extract from side information in the form of an additional feature matrix X' , where we choose Σ_{side} as an RBF kernel on top of the side information X' . Note that this way, the data matrix enters the model both through the linear effect but also through the linear kernel. We evaluate the methods by using n instances of the dataset for training and splitting the remaining examples equally into validation and test sets. This process is repeated 50 times, over which we report on average accuracies or areas under the ROC curve (AUCs) as well as standard errors [17].

The hyperparameters of the kernels, together with the regularization parameter λ_0 , were determined on the validation set, using grid search over a sufficiently large parameter space (optimal values are attained inside the grid; in most cases $\lambda_i \in [0.1, 1000]$). For all datasets, the features were centered and scaled to unit standard deviation, except in experiment 4.4, where the features are binary.

In sections 4.3 and 4.4, we show that including a linear kernel into the covariance matrix leads to top features which are less correlated with the population structure in comparison to the features of uncorrelated probit regression. The correlation plots² in Fig. 4 show the mean correlation of the top features with population structure and the corresponding standard errors.

4.2 Simulated data

We generate synthetic data as follows. We generate a weight vector $w \in \mathbb{R}^{50}$ with $1 \leq k \leq 50$ entries being 1, and the other $50 - k$ entries being 0. We then create a random covariance matrix $\Sigma_{\text{side}} \in \mathbb{R}^{200 \times 200}$, which serves as side information matrix³. We draw 200 points $X = \{x_1, \dots, x_{200}\}$ independently from a uniform distribution over the unit cube $[-1, 1]^{50}$

²The correlation plots in Fig. 4 are created according to [22] as follows. First, we randomly choose 70% of the available data as training set and obtain a weight vector w by training. We compute the empirical Pearson correlation coefficient

of each feature with the first principle component of the linear kernel on top of the data. This is a way to measure the correlation with the population structure [30]. We define the index set I by taking the absolute value of each entry of w and sorting them in descending order. We now sort the so-obtained list of correlation coefficients with respect to the index set I and obtain a resorted list of correlation coefficients (c_1, \dots, c_n) . In the last step, we obtain a new list $(\hat{c}_1, \dots, \hat{c}_n)$ by smoothing the values, computing $\hat{c}_i := \frac{1}{i} \sum_{k=1}^i c_k$. Finally, we plot the values $(\hat{c}_1, \dots, \hat{c}_n)$ with respect to I . This procedure was repeated 30 times for different random choices of training sets.

³The covariance matrix was created as follows. The random generator in MATLAB version 8.3.0.532 was initialized to seed = 20 using the `rng(20)` command. The matrix Σ_{side} was realized in two steps via `A=2*rand(50,200)-1` and `$\Sigma_{\text{side}}=3*A'*A+0.6*\text{eye}(200)+3*\text{ones}(200,200)$` .

and create the labels according to the probit model, Eq. 4, using Σ_{side} as covariance matrix. We reserve 100 samples for training and 50 for validation and testing, respectively. As a benchmark we introduce the *oracle classifier*, where we use the correlated probit model (with covariance matrix Σ_{side}) but skip the training and instead use the true underlying w for prediction.

For several $1 \leq k \leq 50$, we generate a dataset according to the above described procedure. In Fig. 1, we report on the so-achieved accuracies with respect to the percentage of non-zero features ($\frac{k}{50}\%$). We observe that in the sparse scenarios ($\leq 20\%$ non-zero features), GP classification and LMM-Lasso are clearly outperformed by CPR, achieving an accuracy up to 10 percentage points and 23 percentage points higher, respectively. Due to being ℓ_1 -norm regularized and therefore, having the capability of exploiting sparsity, uncorrelated probit regression performs best in this regime among the competitors, but still substantially worse than CPR. LMM-Lasso is also ℓ_1 -norm regularized but is not designed for a classification setting. Therefore, it cannot beat uncorrelated probit regression. In the dense scenarios, CPR outperforms LMM-Lasso (by 1 to 4 percentage points) and performs similarly well to GP classification, which also takes the correlation structure into account. In this scenario, uncorrelated probit regression is clearly worse than the other methods, because it does not take the correlation structure into account. We observe that in all scenarios the prediction performance of CPR-MAP is between uncorrelated probit regression and CPR.

In Fig. 2, we inspect the computed feature weights (green dots) of ℓ_1 -norm regularized and ℓ_2 -norm regularized CPR, respectively. The blue solid line represents the ground truth (the true underlying weight vector w with $k = 10$ entries non-zero). We observe that the ℓ_1 -norm regularized probit model finds the true weights without suffering from large noise as the ℓ_2 -norm regularized counterpart does.

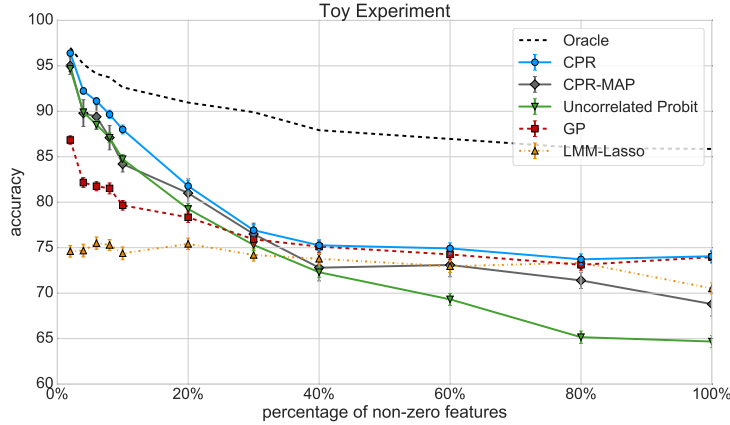


Figure 1: TOY: Average accuracies as a function of the number of true non-zero features in the generating model. (Proposed methods: CPR and CPR-MAP)

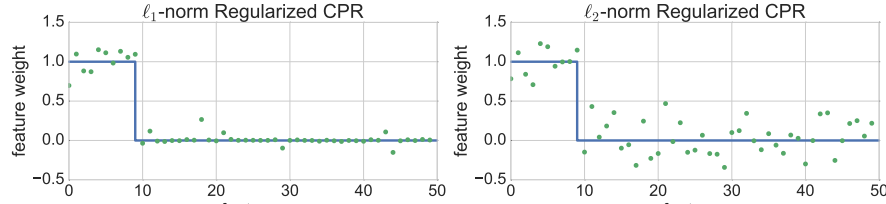


Figure 2: TOY: Ground truth (blue solid line) and feature weights (green dots) of ℓ_1 -norm (LEFT) and ℓ_2 -norm (RIGHT) regularized correlated probit regression.

4.3 Tuberculosis disease outcome prediction from gene expression levels

We obtained the dataset by [4] from the National Center for Biotechnology Information website⁴, which includes 40 blood samples from patients with active tuberculosis as well as 103 healthy controls, together with the transcriptional signature of blood samples measured in a microarray experiment with 48,803 gene expression levels, which serve as features for our purposes. Also available is the age of the subjects when the blood sample was taken, from which we compute Σ_{side} ⁵. All competing methods are trained by using various training set sizes $n \in [40, 80]$. To be consistent with previous studies (e.g. [22]), we report on the area under the ROC curve (AUC), rather than accuracy. The results are shown in Fig. 3, left.

We observe that CPR achieves a consistent improvement over its uncorrelated counterpart (by up to 12 percentage points), GP classification (by up to 3 percentage points), LMM-Lasso (by up to 7 percentage points) and CPR-MAP (by up to 7 percentage points). In Fig. 4, left, we show the correlation of the top features with population structure (as confounding factor) for correlated and uncorrelated probit regression. The plot was created as explained in section 4.1. We find that the features obtained by CPR show much less correlation with population structure than the features of uncorrelated probit regression. By inspecting in the correlation coefficients of the first top 10 features of both methods, we observe that the features found by CPR are 40 % less correlated with the confounder. This is because population structure was built into our model as a source of correlated noise.

4.4 Malicious computer software (malware) detection

We experiment on the Drebin dataset⁶ [1], which contains 5,560 Android software applications from 179 different malware families. There are 545,333 binary features; each feature denotes the presence or absence of a certain source code string (such as a permission, an API call or a network address). It makes sense to look for sparse feature vector [1], as only a small number of strings are truly characteristic of a malware. The idea is that we consider populations of different families of malware when training, and hence correct for the analogue of genetic population structure in this new context, that we call “malware structure”. We concentrate on the top 10 most frequently occurring malware families in the dataset.⁷

⁴<http://www.ncbi.nlm.nih.gov/geo/query/acc.cgi?acc=GSE19491>

⁵We compute Σ_{side} as RBF kernel on top of the side information age using bandwidth $\sigma = 0.2$.

⁶<http://user.informatik.uni-goettingen.de/~darp/drebin/download.html>

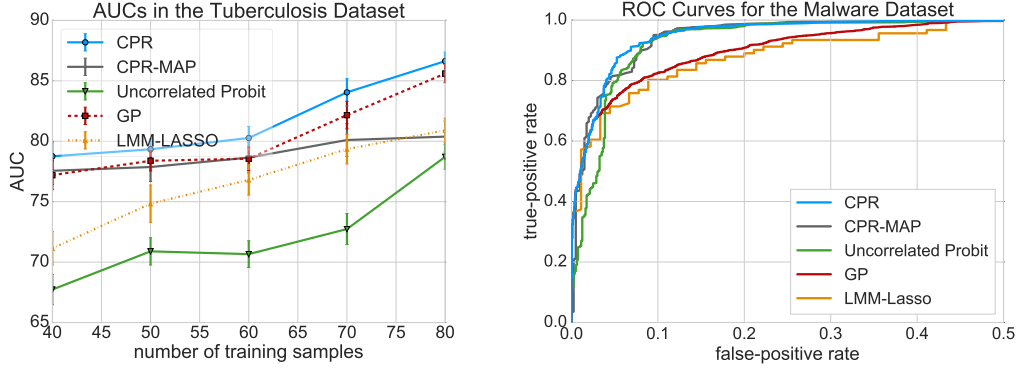


Figure 3: LEFT, TBC: Average AUC in the tuberculosis experiment with respect to the training set size. RIGHT, MALWARE: Average ROC curves for the computer malware detection experiment.

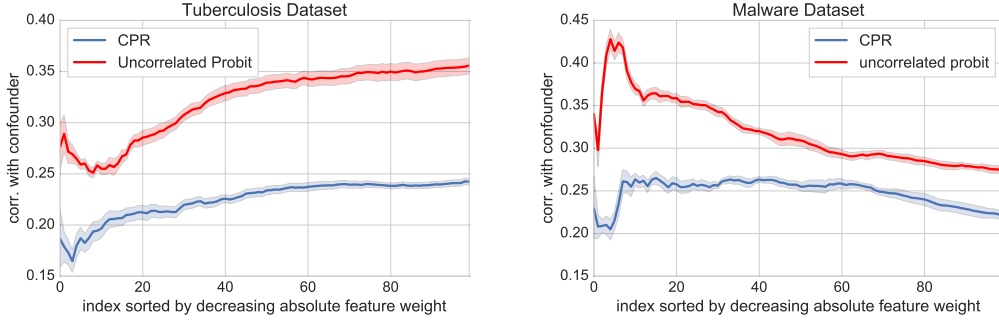


Figure 4: Correlation of the of top features in the tuberculosis experiment (LEFT) and in the computer malware detection experiment (RIGHT). The x-axis is sorted by descending absolute weights.

CPR	CPR-MAP	Uncorr. Probit	GP	LMM-Lasso
74.9 \pm 0.2	73.1 \pm 0.4	67.2 \pm 0.3	69.8 \pm 0.3	66.45 \pm 0.3

Table 1: $AUC_{0.1}$ attained on the malware dataset.

We took 10 instances from each family, forming together a malicious set of 100 and a benign set of another 100 instances (i.e., in total 200 samples). We employ $n = 80$ instances for training and stratify in the sense that we make sure that each training/validation/test set contains 50% benign samples and an equal amount of malware instances from each family. Since no side information is available, we only use a linear kernel and the identity matrix as components for the correlation matrix. We report on the (normalized) area under the Receiver Operating Characteristic (ROC) curve over the interval $[0, 0.1]$ and denote this

⁷Geinimi, FakeDoc, Kmin, Iconosys, BaseBridge, GinMaster, Opfake, Plankton, FakeInstaller, DroidKungFu.

performance measure by $AUC_{0.1}$. In Fig. 3, right, we show the ROC curves and in Table 1 the achieved $AUC_{0.1}$.

We observe that correlated probit regression (CPR) achieves a consistent improvement in terms of $AUC_{0.1}$ over its uncorrelated counterpart (by approximately 7.5 percentage points), GP classification (by approximately 5 percentage points), LMM-Lasso (by approximately 8.4 percentage points) and over CPR-MAP (by approximately 2 percentage points). Furthermore, in Fig. 4, right, we plot the correlation of the top features of correlated and uncorrelated probit regression with population structure. We observe that CPR leads to features, which are much less correlated with the malware structure.

4.5 Flowering time prediction from single nucleotide polymorphisms

We experiment on genotype and phenotype data consisting of 199 genetically different samples from the model plant *Arabidopsis thaliana* [3]. The genotype of each sample comprises 216,130 single nucleotide polymorphism (SNP) features. The phenotype that we aim to predict is early or late flowering of a plant when grown at ten degrees centigrade. The original dataset contains the flowering time for each of the 199 genotypes. We split the dataset into the lower and upper 45%-quantiles of the flowering time and binarized the labels, resulting in a set of 180 instances from which we use $n = 150$ instances for training. The results are

CPR	CPR-MAP	Uncorr. Probit	GP	LMM-Lasso
84.1 ± 0.2	83.6 ± 0.3	83.5 ± 0.2	83.6 ± 0.2	79.7 ± 0.2

Table 2: FLOWERING time prediction experiment (AUCs).

reported in Table 2 and show that CPR has a slight advantage of at least 0.5 percentage points in AUC over the competitors.

An analysis restricted to the ten SNPs with largest absolute regression weights in our model showed that they lie within four well-annotated genes that all convincingly can be related to flowering, structure and growth: the gene AT2G21930 is a growth protein that is expressed during flowering, AT4G27360 is involved in microtubule motor activity, AT3G48320 is a membrane protein, involved in plant structure, and AT5G28040 is a DNA binding protein that is expressed during flowering.

5 Related Work

We have already commented on how our model relates to uncorrelated probit regression, GP classification, and linear mixed models. A common generalized linear model for classification is the logistic regression model [10]. Accounting for correlations in the data is non-straightforward [31]; one has to resort to approximate inference techniques, including the Laplace and mean field approximations that have been proposed in the context of GP classification [33], or the pseudo likelihood method, which has been proposed in the context of generalized linear mixed models [8]. To our knowledge feature selection has not been studied in a correlated logistic setup. On the other hand, without correlations, there is numerous work on feature selection in Lasso regression [35]. Alternative sparse priors to

the Lasso have been suggested in [25] for unsupervised learning (again, without compensating for confounders). The joint problem of sparse estimation in a correlated noise setup has been restricted to the linear regression case [34, 36, 32], whereas we are interested in classification. For classification, we remark that the ccSVM [22] deals with confounding in a different way and it does not yield a sparse solution. Finally, our algorithm builds on EP for GP classification [33, 12], but note that GP classification does not yield sparse estimates and, therefore, gives no insights in the underlying structure of the problem.

6 Conclusion

We presented a novel algorithm for sparse feature selection in binary classification where the training data show spurious correlations due to confounding. Our model is inspired by the linear mixed model of linear regression, where confounding is modeled in terms of a correlated Gaussian noise variable. While generalizing the LMM modeling paradigm to binary classification poses technical challenges as exact inference becomes intractable, our solution relies on approximate inference. We demonstrated the use of our approach on two data sets from the field of statistical genetics; a field plagued by confounding of various sorts.

The algorithm can be seen as a hybrid between an ℓ_1 -norm regularized probit classifier (enforcing sparsity) and a GP classifier that takes as input an arbitrary noise kernel. It distinguishes between sparse linear effects from non-sparse effects due to confounding as modeled in terms of correlated Gaussian noise. We showed that our model selects features that are less correlated with the confounders (defined as the first principal components of the noise covariance) and therefore allows to find effects closer to the truly underlying sparsity pattern.

Finally we remark that there is a certain preoccupation for sparse models in the scientific community due to various reasons. While sparsity by itself is not the ultimate virtue to be strived for, we showed that the combination of sparsity-inducing regularization and dense-type probabilistic modeling (as in the proposed method) may improve over purely sparse models such as ℓ_1 -norm regularized uncorrelated probit regression. The reason for this is less obvious and its theoretical exploration is left for future work. Nevertheless, we remark that a good starting point to this end will be to study the existing literature on compressed sensing as pioneered by [9, 14] and put forward by [6] in the context of 1-bit compressed sensing. For the latter case such theory recently has been developed by [28], but under the assumption of independent noise variables—an assumption that is violated in the correlated probit model.

In the future, several paths are viable. First, a desirable generalization of the method is a multi-class version of the model. Second, one can use the toolbox of Gaussian process classification to automatically adjust the noise covariance from the data. This will make extensive cross-validations superfluous, however, it will also make the problem non-convex. Lastly, a future direction is to make the model even more scalable to massive data sets. To this end, one can make use of the formulation of the model in Eq. 8 and employ Stochastic Variational Inference, a scalable Bayesian algorithm based on stochastic optimization [19]. We will leave this for future studies.

Acknowledgements

We thank Manfred Opper, Mehryar Mohri, David Blei, Rajesh Ranganath, Maja Rudolph, and Gunnar Rätsch for stimulating discussions. SM acknowledges the support of the U.S. National Science Foundation I2CAM International Materials Institute Award, Grant DMR-0844115, and the NSF Schloss Dagstuhl support grant for junior researchers (CNS-1257011). SM and MK gratefully acknowledge the support of the NVIDIA Corporation for the donation of the Tesla K40 GPU. MK acknowledges support from the German Research Foundation (DFG) award KL 2698/2-1.

References

- [1] Arp, D., Spreitzenbarth, M., Hübner, M., Gascon, H., Rieck, K., and Siemens, C. (2014). Drebin: Effective and explainable detection of android malware in your pocket. In *Proc. of NDSS*.
- [2] Astle, W. and Balding, D. J. (2009). Population structure and cryptic relatedness in genetic association studies. *Statistical Science*, pages 451–471.
- [3] Atwell, S., Huang, Y. S., Vilhjálmsson, B. J., Willems, G., Horton, M., Li, Y., Meng, D., Platt, A., Tarone, A. M., Hu, T. T., et al. (2010). Genome-wide association study of 107 phenotypes in arabidopsis thaliana inbred lines. *Nature*, 465(7298):627–631.
- [4] Berry, M. P., Graham, C. M., McNab, F. W., Xu, Z., Bloch, S. A., Oni, T., Wilkinson, K. A., Banchereau, R., Skinner, J., Wilkinson, R. J., et al. (2010). An interferon-inducible neutrophil-driven blood transcriptional signature in human tuberculosis. *Nature*, 466(7309):973–977.
- [5] Bliss, C. I. (1934). The method of probits. *Science*, 79(2037):38–39.
- [6] Boufounos, P. T. and Baraniuk, R. G. (2008). 1-bit compressive sensing. In *Information Sciences and Systems, 2008. CISS 2008. 42nd Annual Conference on*, pages 16–21. IEEE.
- [7] Boyd, S., Parikh, N., Chu, E., Peleato, B., and Eckstein, J. (2011). Distributed optimization and statistical learning via the ADMM. *Foundations and Trends in Machine Learning*, 3(1):1–122.
- [8] Breslow, N. E. and Clayton, D. G. (1993). Approximate inference in generalized linear mixed models. *Journal of the American Statistical Association*, 88(421):9–25.
- [9] Candès, E. J. and Tao, T. (2006). Near-optimal signal recovery from random projections: Universal encoding strategies? *IEEE Transactions Information Theory*, 52(12):5406–5425.
- [10] Cox, D. R. (1958). The regression analysis of binary sequences. *Journal of the Royal Statistical Society. Series B (Methodological)*, pages 215–242.
- [11] Craddock, N., Hurles, M. E., Cardin, N., et al. (2010). Genome-wide association study of cnvs in 16,000 cases of eight common diseases and 3,000 shared controls. *Nature*, 464(7289):713–720.

- [12] Cunningham, J. P., Hennig, P., and Lacoste-Julien, S. (2011). Gaussian probabilities and expectation propagation. *arXiv preprint arXiv:1111.6832*.
- [13] Dempster, A. P., Laird, N. M., and Rubin, D. B. (1977). Maximum likelihood from incomplete data via the em algorithm. *Journal of the royal statistical society. Series B (methodological)*, pages 1–38.
- [14] Donoho, D. L. (2006). Compressed sensing. *IEEE Trans. Inform. Th.*, 52(4):1289–1306.
- [15] Eckstein, J. and Bertsekas, D. P. (1992). On the douglas-rachford splitting method and the proximal point algorithm for maximal monotone operators. *Math. Program.*, 55(3):293–318.
- [16] Fahrmeir, L., Kneib, T., Lang, S., and Marx, B. (2013). *Regression*. Springer.
- [17] Fawcett, T. (2006). An introduction to ROC analysis. *Pattern recognition letters*, 27(8):861–874.
- [18] Fusi, N., Stegle, O., and Lawrence, N. D. (2012). Joint modelling of confounding factors and prominent genetic regulators provides increased accuracy in genetical studies. *PLoS comp. bio.*, 8(1).
- [19] Hoffman, M. D., Blei, D. M., Wang, C., and Paisley, J. (2013). Stochastic variational inference. *The Journal of Machine Learning Research*, 14(1):1303–1347.
- [20] Imbens, G. W. and Rubin, D. B. (2015). *Causal Inference in Statistics, Social, and Biomedical Sciences*. Cambridge University Press.
- [21] Kraft, P., Zeggini, E., and Ioannidis, J. P. (2009). Replication in genome-wide association studies. *Statistical Science: A review journal of the Institute of Mathematical Statistics*, 24(4):561.
- [22] Li, L., Rakitsch, B., and Borgwardt, K. M. (2011). ccsvm: correcting support vector machines for confounding factors in biological data classification. *Bioinformatics*, 27(13):342–348.
- [23] Lippert, C., Listgarten, J., Liu, Y., Kadie, C., Davidson, R., and Heckerman, D. (2011). Fast linear mixed models for genome-wide association studies. *Nature Methods*, 8(10):833–835.
- [24] Manolio, T. A., Collins, F. S., Cox, N. J., Goldstein, D. B., Hindorff, L. A., Hunter, D. J., et al. (2009). Finding the missing heritability of complex diseases. *Nature*, 461(7265):747–753.
- [25] Mohamed, S., Heller, K., and Ghahramani, Z. (2011). Bayesian and l1 approaches to sparse unsupervised learning. *arXiv preprint arXiv:1106.1157*.
- [26] Morgan, S. L. and Winship, C. (2014). *Counterfactuals and causal inference*. Cambridge University Press.
- [27] Pearl, J. et al. (2009). Causal inference in statistics: An overview. *Statistics Surveys*, 3:96–146.
- [28] Plan, Y. and Vershynin, R. (2012). One-bit compressed sensing by lp. *arXiv:1109.4299*.

- [29] Prékopa, A. (1973). On logarithmic concave measures and functions. *Acta Scientiarum Mathematicarum*, 34:35–343.
- [30] Price, A. L., Patterson, N. J., Plenge, R. M., Weinblatt, M. E., Shadick, N. A., and Reich, D. (2006). Principal components analysis corrects for stratification in genome-wide association studies. *Nat Genet*, 38(8):904–909.
- [31] Ragab, A. (1991). On multivariate logistic distribution. *Micro. Reliab.*, 31(2):511–519.
- [32] Rakitsch, B., Lippert, C., Stegle, O., and Borgwardt, K. (2013). A lasso multi-marker mixed model for association mapping with population structure correction. *Bioinformatics*, 29(2):206–214.
- [33] Rasmussen, C. E. and Williams, C. K. I. (2006). *Gaussian Processes for Machine Learning*. MIT Press, Cambridge, MA, USA.
- [34] Seeger, M. W. and Nickisch, H. (2011). Large scale bayesian inference and experimental design for sparse linear models. *SIAM Journal on Imaging Sciences*, 4(1):166–199.
- [35] Tibshirani, R. (1996). Regression shrinkage and selection via the lasso. *Journal of the Royal Statistical Society. Series B (Methodological)*, pages 267–288.
- [36] Vattikuti, S., Lee, J. J., Chang, C. C., Hsu, S. D., and Chow, C. C. (2014). Applying compressed sensing to genome-wide association studies. *GigaScience*, 3(1):10.
- [37] Vilhjálmsson, B. J. and Nordborg, M. (2013). The nature of confounding in genome-wide association studies. *Nature Reviews Genetics*, 14(1):1–2.

A Absorbing the label signs by preprocessing X and Σ

We have claimed in section 2 that without loss of generality, all labels are 1. We will now prove that we can indeed absorb all labels by preprocessing the data matrix. The original problem involves the data matrix $\tilde{X} = (\tilde{X}_1, \dots, \tilde{X}_n) \in \mathbb{R}^{d \times n}$ a vector of observed labels $Y \in \{\pm 1\}^n$, and a noise covariance $\tilde{\Sigma}$. It is $Y = \text{sign}(\tilde{X}^\top w + \tilde{\epsilon})$, $\tilde{\epsilon} \sim \mathcal{N}(0, \tilde{\Sigma})$. We now transform every column of \tilde{X} as $X_i = \tilde{X}_i \circ Y_i$, where \circ is the Hadamard product. When multiplying this equation element-wise with Y , this yields $1 = \text{sign}(X^\top w + Y \circ \tilde{\epsilon})$, $\tilde{\epsilon} \sim \mathcal{N}(0, \tilde{\Sigma})$. Lastly, we observe that the new noise vector $\epsilon = Y \circ \tilde{\epsilon}$ has the effective covariance matrix $\Sigma \equiv \text{diag}(Y) \cdot \tilde{\Sigma} \cdot \text{diag}(Y)$. Hence, after the above transformations, the model reads $1 = \text{sign}(X^\top w + \epsilon)$, $\epsilon \sim \mathcal{N}(0, \Sigma)$. We see that we have effectively absorbed Y by means of a rotation of the data matrix and the noise covariance. This proves our claim.

B Convexity of the Objective

We prove that the objective function Eq. 6 and its MAP approximation Eq. 9 are convex.

We begin by proving convexity of Eq. 6. Since the ℓ_1 -norm regularizer is convex it is sufficient to show that $\mathcal{L}_0(w) \equiv -\log \int_{\mathbb{R}_+^n} \mathcal{N}(\epsilon; X^\top w, \Sigma) d^n \epsilon$ is convex in w . Recall that a function f is log-convex, if f is strictly positive and $\log f$ is convex; log-concavity is defined analogously. In the following, we make use of a theorem that connects log-concave functions to their partial integrals over convex sets [29]. Namely, for a log-concave function $f : \mathbb{R}^{n+m} \rightarrow \mathbb{R}$ and a convex subset $A \subset \mathbb{R}^n$, the function $g(x) = \int_A f(x, y) d^m y$ is log-concave in the entire space \mathbb{R}^n . Since $X^\top w$ is linear, it is sufficient to show that $f(\mu) := -\log \int_{\mathbb{R}_+^n} \mathcal{N}(\epsilon; \mu, \Sigma) d^n \epsilon$ is convex in μ . The multivariate Gaussian density \mathcal{N} is log-concave in $(\epsilon, \mu) \in \mathbb{R}^{2n}$, since $\mathcal{N}(\epsilon; \mu, \Sigma) > 0$ for all $\mu, \epsilon \in \mathbb{R}^n$ and $\log \mathcal{N}$ is concave in (ϵ, μ) . Therefore, $\int_{\mathbb{R}_+^n} \mathcal{N}(\epsilon; \mu, \Sigma) d^n \epsilon$ is log-concave in μ . The logarithm of a log-concave function is concave by definition. Thus, f is convex in μ and therefore, Eq. 6 is convex in w .

Let us now consider the objective function of the MAP approximation, Eq. 9. Since the regularizers are convex in w and w' , it is sufficient to show that $-\sum_{i=1}^n \log \Phi(X_i^\top (w + w') / \sqrt{\lambda_1})$ is convex in $(w, w') \in \mathbb{R}^{2n}$. With analogous arguments showing the convexity of $f(\mu)$, it holds that $g(\mu) := \log \Phi(\frac{\mu}{\sqrt{\lambda_1}})$ is convex in μ . Since $X_i^\top (w + w')$ is linear in (w, w') , it follows that Eq. 9 is convex in (w, w') .

C Predicting new labels

When predicting new labels in the correlated probit regression model, we have two choices. We can either ignore correlations between samples, or take them into account. Both cases have their use which depends on the context. While in the first case we simply take the sign of $X^\top w$ of a new data point to predict its label, the second case closely resembles prediction in Gaussian Processes [33] and shall here be reviewed.

We introduce letters that indicate the training set (R) and the test set (E), and let $y_{E/R}$ be the test and training labels, respectively. We define the mapping $Y_E \mapsto Y := (Y_E^\top, Y_R^\top)^\top \in \mathbb{R}^{m+n}$. We also concatenate test data and training data as $X = (X_E^\top, X_R^\top)^\top \in \mathbb{R}^{d \times (m+n)}$.

$\mathbb{R}^{d \times (m+n)}$. Finally, we consider the concatenated kernel matrices

$$K^i = \begin{pmatrix} K_{EE}^i & K_{ER}^i \\ K_{RE}^i & K_{RR}^i \end{pmatrix} \in \mathbb{R}^{(m+n) \times (m+n)} \quad (17)$$

We use the weights λ_i that were determined by model selection on the training data (Y_R, X_R) to construct the covariance matrix on the extended space, $\Sigma = \sum_i \lambda_i K^i$. In order to predict new labels Y_E , we evaluate the objective, using X , $Y = Y(Y_E)$ and the training weights w . The predicted label is then $Y_E^* = \arg \min_{Y_E \in \{\pm 1\}^m} \mathcal{L}(w|X, Y, \Sigma)$.

D Gradient and Hessian

In this section, we calculate the gradient and the Hessian of the un-regularized objective, $\mathcal{L}_0(w) = -\log \int_{\mathbb{R}_+^n} \mathcal{N}(\epsilon; \mu(w), \Sigma) d^n \epsilon$. It will be sometimes more convenient to consider the objective as a function of $\mu = X^\top w$, rather than w , for which case we define $\mathcal{L}_0(\mu) = -\log \int_{\mathbb{R}_+^n} \mathcal{N}(\epsilon; \mu, \Sigma) d^n \epsilon$. We begin by computing the gradient. We define $\mu_p = \mathbb{E}_{p(\epsilon|\mu, \Sigma)}[\epsilon]$ as the mean of the truncated Gaussian. The gradient is given by

$$\nabla_w \mathcal{L}_0(w) = \frac{\int_{\mathbb{R}_+^n} (\epsilon - \mu)^\top \Sigma^{-1} \mathcal{N}(\epsilon; \mu, \Sigma) d^n \epsilon}{\int_{\mathbb{R}_+^n} \mathcal{N}(\epsilon; \mu, \Sigma) d^n \epsilon} X^\top = (\mu_p - \mu)^\top \Sigma^{-1} X^\top.$$

We now compute the Hessian. We first consider the Hessian matrix of $\mathcal{L}_0(\mu)$, $B_{ij}(\mu) = \partial_{\mu_i} \partial_{\mu_j} \mathcal{L}_0(\mu)$. The chain rule relates this object to the Hessian of $\mathcal{L}_0(w)$, namely $H(w) = X B(\mu) X^\top$. The problem therefore reduces to calculating $B(\mu)$ which is $n \times n$, whereas the original Hessian $H(w)$ is $d \times d$.

To calculate $B(\mu)$, we define $I(\mu) = \int_{\mathbb{R}_+^n} \exp\{-\frac{1}{2}(\epsilon - \mu)^\top \Sigma^{-1}(\epsilon - \mu)\} d^n \epsilon$. Up to a constant, $\mathcal{L}_0(\mu) = -\log I(\mu)$. The Hessian is given by $B_{ij}(\mu) = -\frac{\partial_{\mu_i} \partial_{\mu_j} I(\mu)}{I(\mu)} + \frac{\partial_{\mu_i} I(\mu)}{I(\mu)} \frac{\partial_{\mu_j} I(\mu)}{I(\mu)}$. Note that this involves also the first derivatives of $I(\mu)$, that we have already calculated for the gradient. To proceed, we still need to calculate $\partial_{\mu_i} \partial_{\mu_j} I(\mu)$. To simplify the calculation, we introduce $\tilde{\mu} = \epsilon - \mu$. As a consequence, $\partial_{\tilde{\mu}_i} = -\partial_{\mu_i}$. Furthermore,

$$\partial_{\mu_i} \partial_{\mu_j} \exp\{-\frac{1}{2}(\epsilon - \mu)^\top \Sigma^{-1}(\epsilon - \mu)\} = [\Sigma^{-1} \tilde{\mu} \tilde{\mu}^\top \Sigma^{-1} - \Sigma^{-1}]_{ij} \exp\{-\frac{1}{2}\tilde{\mu}^\top \Sigma^{-1} \tilde{\mu}\}.$$

Based on this identity, we derive $\frac{\partial_{\mu_i} \partial_{\mu_j} I(\mu)}{I(\mu)} = (\Sigma^{-1} \Sigma_p \Sigma^{-1} - \Sigma^{-1})_{ij}$. For the remaining terms, we use our known result for the gradient, namely

$$\frac{\partial_{\mu} I(\mu)}{I(\mu)} = (\mathbb{E}_{p(\epsilon|\mu)}[(\mu_p - \mu)^\top \Sigma^{-1}]) = (\mu_p - \mu)^\top \Sigma^{-1}.$$

As a consequence,

$$\frac{\partial_{\mu_i} I(\mu)}{I(\mu)} \frac{\partial_{\mu_j} I(\mu)}{I(\mu)} = (\Sigma^{-1} \Delta \mu \Delta \mu^\top \Sigma^{-1})_{ij}.$$

Above we defined $\Delta \mu = (\mu - \mu_q)$. This lets us summarize the Hessian matrix $B(\mu)$:

$$B(\mu) = [\Sigma^{-1}(\Sigma_p - \Delta \mu \Delta \mu^\top) \Sigma^{-1} - \Sigma^{-1}] \quad (18)$$

This gives us the Hessian.

Hessian inversion formula. For the second order gradient descent scheme, we need to compute the inverse matrix of the Hessian $H(w)$. Let us call $D = \lambda_0 \mathbf{I}_n$ the (diagonal) Hessian of the regularizer. We use the Woodbury matrix identity,

$$\begin{aligned}
H^{-1} &= (D + XBX^\top)^{-1} \\
&= D^{-1} - D^{-1}X(B^{-1} + X^\top D^{-1}X)^{-1}X^\top D^{-1} \\
&= \lambda_0^{-1} \mathbf{I}_n \lambda_0^{-2} X(B^{-1} + \lambda_0^{-1} X^\top X)^{-1} X^\top.
\end{aligned} \tag{19}$$

Note that this identity does not require us to invert a $d \times d$ matrix, but only involves the inversion of $n \times n$ matrices (in our genetic applications, the number of samples n is typically in the hundreds, while the number of genetic features d is of order $10^4 - 10^5$). We first precompute the linear kernel $X^\top X$. We also use the fact that we can more efficiently compute the product $H^{-1} \nabla_w \mathcal{L}$ as opposed to first calculating the Hessian inverse and then multiplying it with the gradient.